Neuron
Article

Inhibitory Control of Linear and Supralinear Dendritic Excitation in CA1 Pyramidal Neurons

Christina Müller,[1,4] Heinz Beck,[2,4] Douglas Coulter,[3] and Stefan Remy[1,4,*]
[1]NRW Research Group "Dendritic Integration in the CNS"
[2]Laboratory of Experimental Epileptology and Cognition Research
Department of Epileptology, University of Bonn, Sigmund-Freud-Straße 25, 53105 Bonn, Germany
[3]Departments of Pediatrics and Neuroscience, University of Pennsylvania School of Medicine, and the Children's Hospital of Philadelphia, Abramson Pediatric Research Center, 3615 Civic Center Boulevard, Philadelphia, PA 19104-4318, USA
[4]Deutsches Zentrum für Neurodegenerative Erkrankungen e.V. (DZNE), Ludwig-Erhard-Allee 2, 53175 Bonn, Germany
*Correspondence: stefan.remy@dzne.de
http://dx.doi.org/10.1016/j.neuron.2012.06.025

SUMMARY

The transformation of dendritic excitatory synaptic inputs to axonal action potential output is the fundamental computation performed by all principal neurons. We show that in the hippocampus this transformation is potently controlled by recurrent inhibitory microcircuits. However, excitatory input on highly excitable dendritic branches could resist inhibitory control by generating strong dendritic spikes and trigger precisely timed action potential output. Furthermore, we show that inhibition-sensitive branches can be transformed into inhibition-resistant, strongly spiking branches by intrinsic plasticity of branch excitability. In addition, we demonstrate that the inhibitory control of spatially defined dendritic excitation is strongly regulated by network activity patterns. Our findings suggest that dendritic spikes may serve to transform correlated branch input into reliable and temporally precise output even in the presence of inhibition.

INTRODUCTION

In all principal neurons of the central nervous system the integration of excitatory inputs is powerfully controlled by the activation of inhibitory GABAergic microcircuits. The diversity of GABAergic interneurons enables them to provide layer-specific and activity-dependent inhibition onto principal neurons (Ali et al., 1998; Ali and Thomson, 1998; Freund and Buzsáki, 1996; McBain and Fisahn, 2001; Pouille and Scanziani, 2004; Somogyi and Klausberger, 2005; Stokes and Isaacson, 2010). This is particularly true for recurrent inhibition in the CA1 hippocampal subfield (Pouille and Scanziani, 2004). There, recurrent dendritic inhibition is provided by several interneuron subtypes including bistratified cells (90% of the synapses are formed on small dendrites), basket cells (40%–50%), and OL-M cells (more than 90% on small apical tuft dendrites) (Földy et al., 2010; Halasy et al., 1996; Somogyi and Klausberger, 2005). Until now, mainly computational models and only few physiological experiments have addressed how inhibition affects integration of excitatory signals on dendrites (Ferster and Jagadeesh, 1992; Hao et al., 2009; Koch et al., 1983; Miles et al., 1996).

Therefore, a major goal of this study was to experimentally resolve how recurrent inhibition controls linear and nonlinear dendritic integration. CA1 pyramidal neuron dendrites are capable of at least two different integration modes: If the spatio-temporal clustering of inputs is low, excitatory postsynaptic potentials on dendritic branches sum linearly, whereas at higher input synchrony, local supralinear dendritic Na^+ spikes can be initiated (Gasparini et al., 2004; Losonczy and Magee, 2006; Remy et al., 2009; Stuart et al., 1997). These dendritic spikes exhibit several functions: dendritic spikes have been shown to serve as efficient triggers of axonal action potentials (AP) with high temporal precision (Ariav et al., 2003; Golding and Spruston, 1998; Losonczy and Magee, 2006; Losonczy et al., 2008; Milojkovic et al., 2004). In addition, dendritic spikes have been implicated in hippocampal mnemonic functions by providing dendritic calcium influx and depolarization sufficient to induce synaptic plasticity (Golding et al., 2002; Holthoff et al., 2004; Remy and Spruston, 2007). Finally, the strength of a dendritic spike on a particular dendritic branch has been shown to undergo activity- and experience-dependent plasticity (Losonczy et al., 2008; Makara et al., 2009). However, the functional interaction of dendritic NA^+ spikes and inhibitory GABAergic microcircuits is so far completely unknown. Therefore, it is important to resolve how dendritic spikes could maintain their specific signaling functions, while interacting with an activity-dependent inhibitory micronetwork.

The central question of this study is how linear and nonlinear excitatory signals in CA1 dendrites are controlled by recurrent inhibition. We coactivated excitation and inhibition by simultaneously using branch-targeted microiontophoresis of glutamate together with either selective electrical stimulation of CA1 recurrent inhibitory microcircuits or local GABA microiontophoresis. We demonstrate that correlated excitatory input on highly excitable dendritic branches can resist recurrent inhibitory control by initiating strong dendritic spikes, whereas inputs on other branches are subjected to powerful and dynamic regulation by inhibition. Moreover, potentiation of branch excitability serves to achieve effective coupling of branch input to precisely triggered action potential output, independent of recurrent inhibition.

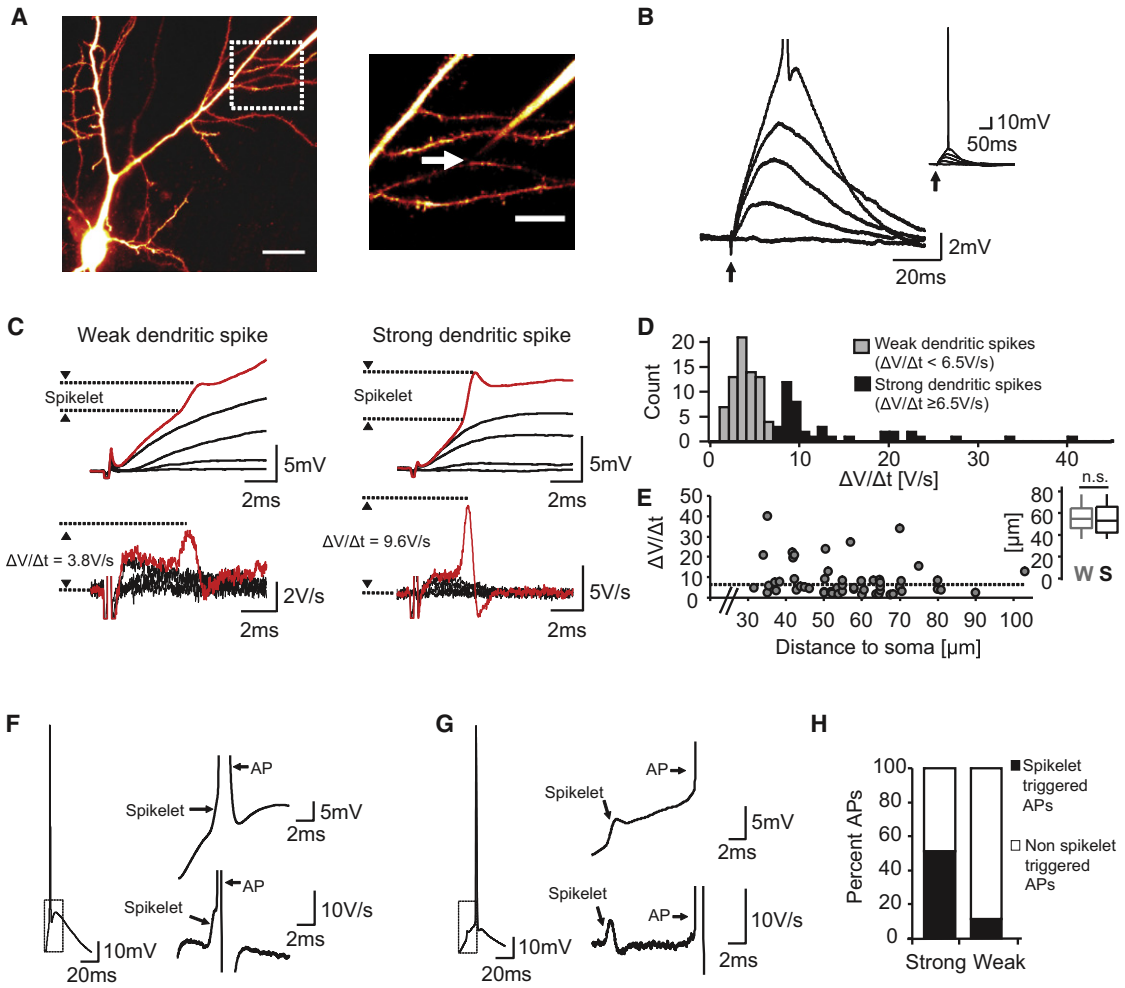

Figure 1. Spatially Defined Sub- and Suprathreshold Dendritic Excitation Evoked by Glutamate Microiontophoresis

(A) Two-photon maximal intensity projection of an image stack showing a CA1 pyramidal neuron filled with Alexa 594 (50 μM) via the patch pipette. Scale bar represents 25 μm. Right: higher magnification. The arrow indicates the position of the microiontophoresis pipette on an apical oblique dendrite (glutamate concentration: 250 mM); scale bar represents 10 μm.

(B) Iontophoretic EPSPs (iEPSPs) and action potential (AP) evoked by increasing iontophoretic current (0–180 pA). The arrow indicates the time point of iontophoretic stimulation (stimulus duration 0.4 ms). Inset: full scale.

(C) Left: microiontophoresis on a weakly excitable branch: iEPSP amplitudes increased with iontophoretic current until the threshold for the dendritic spike initiation was crossed (red trace: weak dendritic spike). Lower traces: corresponding ΔV/Δt. Right: microiontophoresis on a highly excitable branch: representative iEPSPs, a strong dendritic spike (red trace) and corresponding ΔV/Δt traces (lower panel).

(D) Histogram of the dendritic spike ΔV/Δt evoked by iontophoresis on basal and oblique dendrites (n = 113 branches; bin size = 1 V/s).

(E) Anatomical distribution of distances from soma to microiontophoretic stimulation sites (n = 53 branches; 31 exhibiting weak spikes and 22 strong spikes). Dotted line indicates 6.5 V/s. Inset: box plot shows the median and quartiles of stimulation site to soma distances for weak and strong spikes ($p > 0.05$; unpaired t test).

(F) Example of spikelet-triggered AP (left). Magnification and corresponding ΔV/Δt (right).

(G) Example of an AP triggered by the slow component following the spikelet (left). Magnification and corresponding ΔV/Δt (right).

(H) Probability of evoking spikelet-triggered APs for strong (n = 11 branches) and weak dendritic spikes (n = 14 branches).

See also Figures S1, S2, and S3.

RESULTS

Spatially Defined Dendritic Excitation Using Glutamate Microiontophoresis

To examine the interaction of dendritic excitation and inhibition it is necessary to evoke spatially defined excitation. We achieved this by using glutamate microiontophoresis locally on dendritic branches of CA1 pyramidal neurons (Figure 1A; Figures S2A and S2B available online; see also Experimental Procedures). Systematically increasing the iontophoretic current caused somatic EPSPs (iEPSPs) of increasing amplitude, which ultimately triggered action potentials (Figure 1B). The iEPSPs initially increased linearly in all branches, but a subset of basal and apical oblique dendrites exhibited supralinear dendritic

spikes (Figure 1C). Supralinear events were not observed when microiontophoretic stimulation was applied to apical tuft dendrites (n = 42 branches; Figure S3). In the somatic recording, the dendritic spike manifested as a fast spikelet riding on the iEPSP followed by a slower NMDA receptor and voltage gated Ca^{2+} channel dependent component (Losonczy and Magee, 2006). The fast spikelet could be easily detected as a sudden increase of the first derivative of the voltage signal ($\Delta V/\Delta t$; Figure 1C, lower traces). The latencies of the fast spikelet components did not differ significantly between weak (median latency 4.5 ± 2.6 ms SD; n = 186 dendritic spikes) and strong dendritic spikes (median latency 3.9 ± 2.2 ms SD, n = 185 dendritic spikes; $p > 0.05$; Mann-Whitney test, data not shown); yet, weak dendritic spikes showed higher temporal jitter (F-test, data not shown).

We observed a two-peaked distribution of branch excitability with two populations of dendritic spikes that could be separated according to the maximum of the first derivative ($\Delta V/\Delta t$; weak spikes: $\Delta V/\Delta t < 6.5$ V/s, n = 69; strong spikes: $\Delta V/\Delta t \geq 6.5$ V/s, n = 44; Figure 1D). We found no differences in the distribution of dendritic spike $\Delta V/\Delta t$ according to the distances between the soma and the iontophoretic stimulation site, where the dendritic spike was evoked (Figure 1E). Such a distribution has been previously described in CA1 pyramidal neurons using two-photon uncaging of MNI-glutamate (Losonczy et al., 2008; Remy et al., 2009). The time course and amplitude of dendritic spikes evoked by microiontophoresis, focal synaptic stimulation or two-photon uncaging of MNI-caged-glutamate were virtually identical (Figure S1). The spatial extent of a single microiontophoretic stimulation was approximately 12 μm (Figure S2). Using glutamate microiontophoresis dendritic spikes could be reliably elicited for up to 260 times without detectable dendritic damage and glutamate toxicity.

Both strong and weak dendritic spikes have been shown to serve as efficient triggers of neuronal action potential output (Antic et al., 1999; Ariav et al., 2003; Losonczy and Magee, 2006; Remy et al., 2009; Schiller et al., 2000). In our experiments dendritic spikes efficiently triggered action potentials with either the fast Na^+ spikelets, resulting in temporally precise output (Figure 1F; median latency: 5.4 ± 2.9 ms SD; n = 60 APs, data not shown), or with the slower NMDAR- and Ca^{2+} channel-dependent component following the spikelet (Gasparini et al., 2004), resulting in a temporally more imprecise action potential firing (Figure 1G; median latency: 12.8 ± 3.1 ms SD; n = 191 APs, data not shown). When we evaluated which triggering mode was predominantly employed by either weak or strong dendritic spikes we found that strong dendritic spikes predominantly contributed to fast spikelet-triggered output (82% of all spikelet-triggered APs), whereas weak dendritic spikes were more likely to trigger action potentials with the slow depolarization following the spikelet (18% of spikelet-triggered APs; Figure 1H).

Potent Recurrent Inhibition of EPSPs and Weak Dendritic Spikes

Next, we investigated the interaction of EPSPs and recurrent inhibition. Therefore, recurrent inhibitory micronetworks were activated by stimulating CA1 axons in the alveus with a burst stimulus (three stimuli at 100 Hz; Figure 2A; see Experimental Procedures), resulting in an IPSP consisting of three components (Figure 2A, right panel). We evoked iEPSPs of increasing amplitudes on proximal (basal and apical oblique) dendrites together with IPSPs of constant amplitudes (Figure 2B). A single burst stimulus delivered to the alveus significantly reduced the somatically recorded iEPSP (Figure 2B, mean amplitude of subthreshold iEPSPs: 4.5mV ± 0.1mV, with inhibition: 2.6mV ± 0.2mV). When we recorded iEPSP-associated Ca^{2+} transients on the stimulated branch, we observed a significant reduction of the peak Ca^{2+} transient by recurrent inhibition (Figure 2C).

To quantify inhibitory effects on action potential output we adjusted the size of the iEPSPs to obtain an 80%–90% probability of action potential firing. As expected, recurrent inhibition strongly reduced the firing probability of CA1 pyramidal neurons (to 14% ± 5%; Figure 2D).

The generation of fast dendritic spikes has emerged as a key mechanism to amplify synchronous and spatially clustered inputs and to convert them to action potential output (Losonczy et al., 2008). However, how these events are controlled by inhibition is so far unknown. Using the experimental paradigm introduced above, we found that initiation of weak dendritic spikes was reliably suppressed by recurrent inhibition (control dendritic spike probability: 83% ± 4%, with inhibition: 40% ± 8%; Figures 3A, left panel, and 3B). In the presence of inhibition, reinitiating dendritic spikes was possible, but required ~30% higher stimulus intensities (Figures 3C, left panel, and 3D). This block of weak dendritic spiking was detected at timings relevant for recurrent inhibition (onset of inhibition with a disynaptic delay: t_0, see Experimental Procedures), but also when excitation occurred at later time points closer to the peak of inhibition (20 ms delay: t_1; Figures 3E and 3F). When excitation occurred after the IPSP peak (50 ms delay: t_2) no significant block of dendritic spiking could be observed (Figures 3E and 3F).

Resistance of Strong Dendritic Spikes to Inhibition

Remarkably, and in contrast to weak dendritic spikes, strong dendritic spikes consistently resisted recurrent inhibition (control dendritic spike probability: 84% ± 3%, plus inhibition: 78% ± 4%; n = 11 dendritic branches, Figures 3A right panel, 3B, 3C, right panel, and 3D). This pronounced resistance was present at all time delays studied (Figures 3G and 3H). We asked whether this difference between highly and weakly excitable branches was still present when branch inhibition was not limited to recurrent inhibitory synapses. We therefore induced a maximal branch inhibition by local activation of GABA receptors using microiontophoresis of GABA (which activated receptors belonging to recurrent and feedforward synapses). At the same time, on either weakly or highly excitable branches, dendritic spikes were evoked with a second microiontophoretic pipette containing glutamate (Figure 4A). When a dendritic spike was paired with the iontophoretic IPSP (iIPSP) we found a similar selective block of weak dendritic spiking as with synaptic activation of recurrent microcircuits (Figure 4B). However, strong dendritic spikes could still be reliably initiated (Figure 4C), confirming that the resistance of strong spikes is a generalizable phenomenon that is not limited to recurrent GABAergic inhibition.

Why are strong spikes less affected by recurrent inhibition? One likely hypothesis is that the additional excitation provided

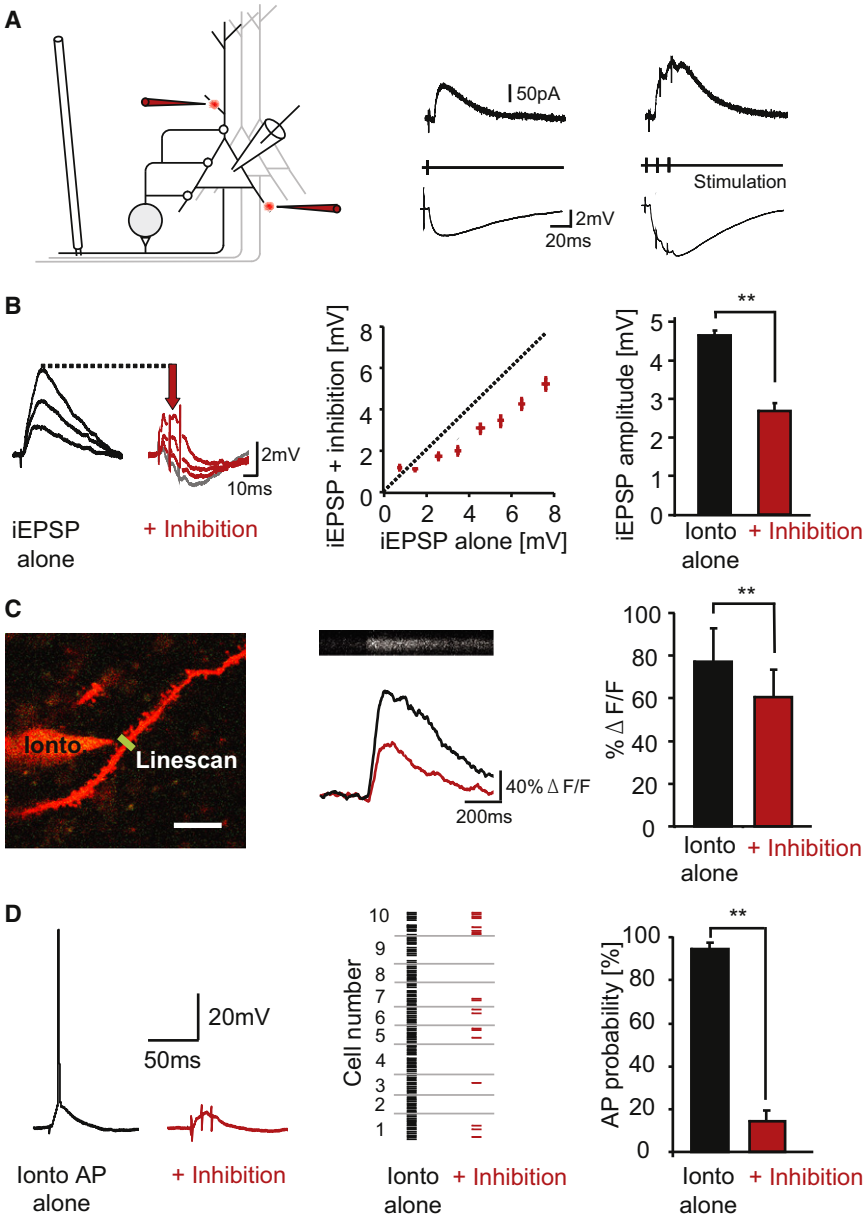

Figure 2. Recurrent Inhibition of iEPSPs, iEPSP-Associated Ca^{2+} Transients, and APs

(A) Schematic recording configuration: whole-cell recording of CA1 pyramidal neurons. Red electrodes represent locations on proximal (basal and apical oblique) dendrites, where excitatory events were evoked with microiontophoresis. Stimulating the alveus evoked recurrent inhibition. Right: single or burst stimulation of the alveus evoked prominent recurrent IPSCs (voltage clamp, upper traces) and IPSPs (current clamp, lower traces) in CA1 pyramidal neurons.

(B) Example traces showing increasing iEPSP amplitudes evoked on proximal dendrites by increasing iontophoretic currents, alone (black) and with recurrent inhibition (red; gray trace indicates IPSP alone). Middle: input-output relation of n = 18 branches (dotted line: angle bisector); mean ± SEM. Right: mean iEPSPs of defined amplitudes alone (black) and with inhibition (41% reduction in amplitude, $p < 0.01$; ANOVA, Dunnett's post hoc test, compare to Figure S7); mean ± SEM.

(C) Left: positioning of iontophoretic pipette for two-photon Ca^{2+}-imaging on a dendritic branch (filled with 50 μM Alexa 594 and 200 μM OGB-1; scale bar represents 8.3 μm; green line indicates positioning of line scan). Middle: iontophoretically evoked Ca^{2+}-signal on a proximal dendrite alone (black) and with recurrent inhibition (red). Right: reduction of Ca^{2+}-signals locally on the dendrite (n = 9 dendritic branches; $p < 0.01$; Wilcoxon signed rank test); mean ± SEM.

(D) Left: representative example of an AP evoked by microiontophoresis on a proximal branch alone and with recurrent inhibition. Middle: effect of recurrent inhibition on microiontophoresis-evoked AP output in n = 10 cells. Right: mean firing probabilities of evoked APs alone (black) and with recurrent inhibition (red; n = 10 cells; $p < 0.001$; Friedman test and Dunn's post hoc test); mean ± SEM.

by downregulation of A-type potassium channels in strong branches increases the probability for excitatory input to bypass the voltage gap provided by dendritic inhibition. To find out if additional mechanisms exist, we tested whether recurrent inhibition of subthreshold EPSPs is altered on weakly and strongly excitable branches (iEPSPs on weak branches: 4.1mV ± 0.3mV, n = 10, strong branches: 4.1mV ± 0.4mV, n = 6). Somatic IPSP amplitudes were identical in both experimental groups (−2.7mV ± 0.3mV and −2.6mV ± 0.3mV; $p > 0.05$; unpaired t test). Interestingly, we found that the subthreshold iEPSPs were significantly less inhibited on branches giving rise to strong dendritic spikes compared to the iEPSPs on weak dendritic branches (51% ± 4% inhibition of iEPSPs on weak branches compared to 26% ± 7% inhibition on strong branches; Figure 4D).

Can this finding be explained by a lower density of GABAergic receptors on branches that give rise to strong spikes? To address this question, we analyzed the slopes of input-output relations for GABA microiontophoresis on selected branches. We did not observe significant differences between weakly and highly excitable branches, suggesting an equal density of available GABA receptors on both branch types (mean slope for weak branches: −2.46mV ± 0.66mV × μA^{-1}, n = 7, strong: −2.28mV ± 1.14mV × μA^{-1}, n = 6; $p > 0.05$; unpaired t test; Figure 4E).

In addition, we tested whether differences in the GABA reversal potential (E_{GABA}) existed between weak and strong branches (Figure 4F). Again, we could not observe a branch-specific difference in E_{GABA} (weak branches: −68.26mV ± 2.94mV; n = 6; strong branches: −67.16mV ± 1.12mV; n = 7; $p > 0.05$; unpaired t test).

Taken together, a subset of branches that generated strong Na^+ spikes was significantly more resistant to inhibition than

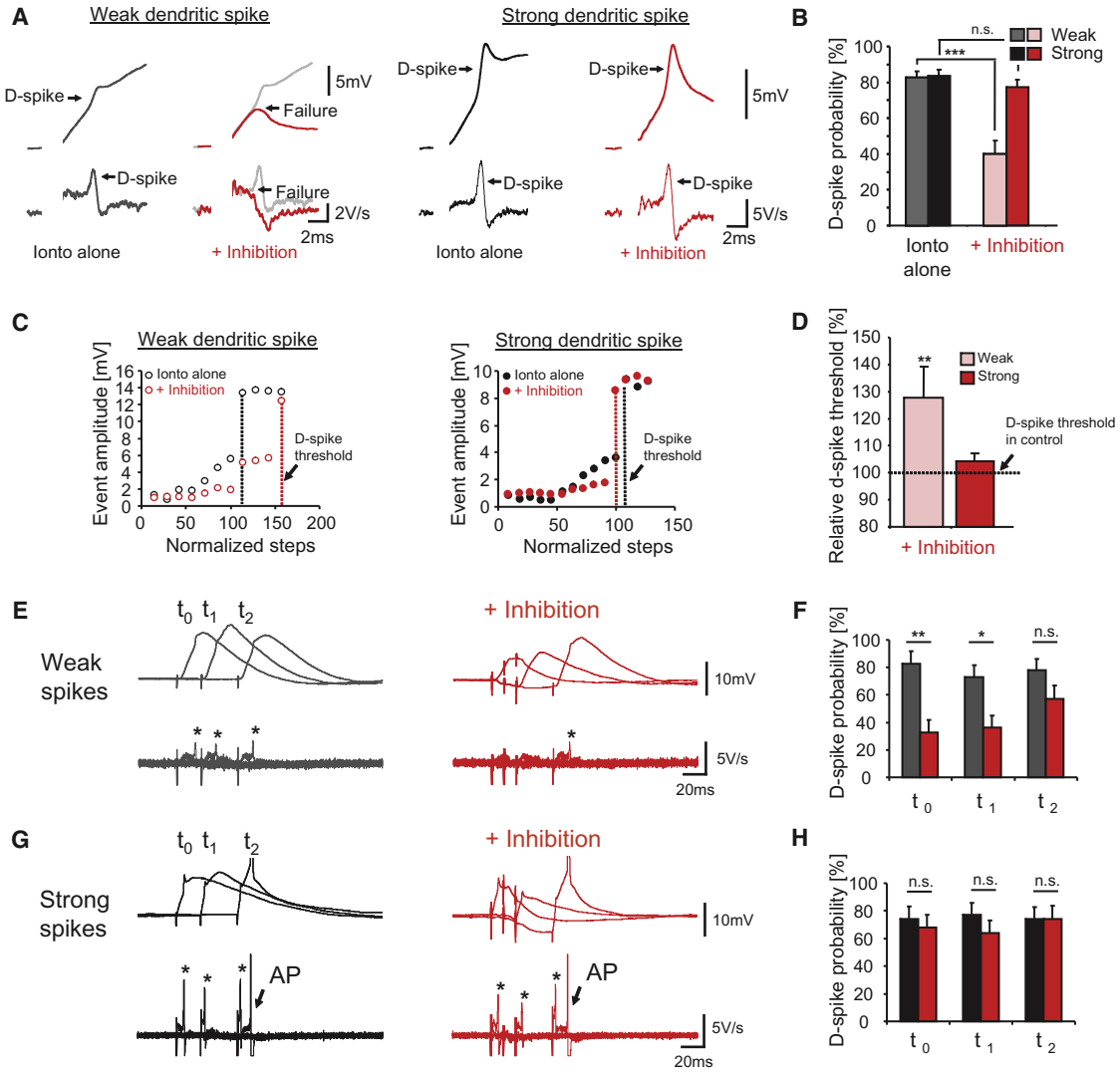

Figure 3. Recurrent Inhibition of Weak and Strong Dendritic Spikes: Strong Dendritic Spikes Resist Recurrent Inhibition

(A) Left: example of a weak dendritic spike alone (black) and with recurrent inhibition (red). Right: example of a strong dendritic spike alone (black) and with recurrent inhibition (red).

(B) Dendritic spike probabilities (pale bars: n = 14 weak dendritic spikes; bright bars: n = 11 strong dendritic spikes) alone (black) and with recurrent inhibition (red; $p < 0.001$, Friedman and Dunn's post hoc test); mean ± SEM.

(C) Left: input-output relation of a weak dendritic spike alone (black open circles) and with recurrent inhibition (red open circles). Right: input-output relation of a strong dendritic spike alone (black solid circles) and with recurrent inhibition (red solid circles).

(D) Stimulus strength required to elicit a dendritic spike in the presence of inhibition compared to control conditions ($p < 0.01$; n = 11 weak and n = 6 strong spikes; Friedman/Dunn's test); mean ± SEM.

(E–H) Probability of dendritic spike generation compared to control conditions determined at three different timings of recurrent inhibition. t_0: Inhibition and excitation are evoked at the same time, resulting in recurrent inhibition occurring with a physiological disynaptic delay. t_1 and t_2: Excitation is evoked with a 20 ms or 50 ms delay, respectively. (E) Example of weak dendritic spikes alone (gray) and with recurrent inhibition evoked at the three different timings (red). Lower traces show corresponding $\Delta V/\Delta t$, asterisks indicate dendritic spikes. (F) Dendritic spike probability alone and with inhibition at three different timings (n = 7 branches; $p < 0.01$; $p < 0.05$; $p > 0.05$; Friedmann/Dunn's test); mean ± SEM. (G) As in (E) for strong dendritic spikes. (H) Dendritic spike probability alone and with inhibition at the three different timings (n = 6 branches; $p > 0.05$; Friedmann/Dunn's test); mean ± SEM.

branches generating weak spikes. Differences observed in recurrent inhibition of subthreshold iEPSPs between strongly and weakly excitable branches could be attributed to neither branch-specific differences in the density of GABA receptors nor a different GABA reversal potential.

Effects of Selective Dendritic Spike Inhibition on Action Potential Probability

Dendritic spikes are able to trigger temporally precise action potential output (Figures 1F and 1G). Thus, we next asked how recurrent inhibition affects the generation of dendritic

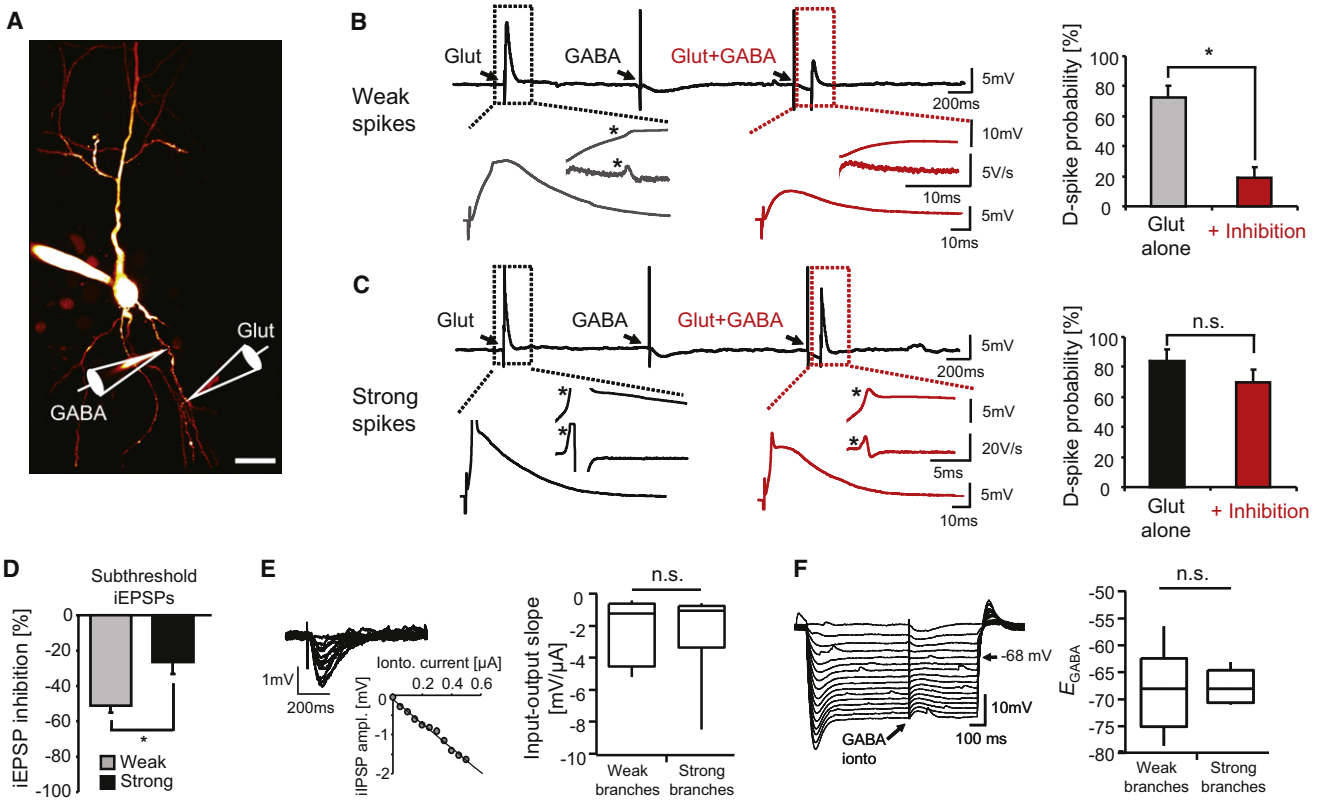

Figure 4. Simultaneous GABA and Glutamate Iontophoresis Reveals Resistance of Strong Dendritic Spikes

(A) Two-photon maximal intensity projection of an image stack showing a CA1 pyramidal neuron filled with Alexa 594 (100 μM; scale bar represents 20 μm), schematic pipettes indicate locations of microiontophoretic stimulation.

(B) Representative recording: first glutamate iontophoresis alone (black), evoking a weak dendritic spike; GABA iontophoresis alone, evoking an iIPSP and both together (red). Lower traces: magnifications and $\Delta V/\Delta t$, asterisks indicate dendritic spike. Right: weak dendritic spike probability alone and with GABA-iontophoretic inhibition ($n = 6$; $p < 0.05$; Wilcoxon signed rank test); mean ± SEM.

(C) As in (B) for strong dendritic spikes ($n = 8$; $p > 0.05$; Wilcoxon signed rank test); mean ± SEM.

(D) Inhibition of subthreshold iEPSPs evoked on identified weakly excitable and strongly excitable branches (all branches included here exhibited dendritic spikes). Weakly excitable branches are more inhibited than strongly excitable branches ($p < 0.05$; $n = 10$ weak and $n = 6$ strong branches; Mann-Whitney test); mean ± SEM.

(E) Left: input-output curve of iIPSPs in response to increasing iontophoretic currents; inset: corresponding voltage traces. Right: slope of input-output relation of iIPSPs evoked on weak and strong branches ($p > 0.05$; $n = 8$ weak and $n = 6$ strong branches; unpaired t test); median ± SD.

(F) Somatic current injections and GABA microiontophoresis on a branch, arrow indicates GABA reversal potential (E_{GABA}). Right: E_{GABA} for iIPSPs evoked on weakly or highly excitable branches ($n = 6$ and $n = 7$, respectively; $p > 0.05$; unpaired t test); median ± SD.

spike-triggered action potential output. We confirmed the specialized role of strong dendritic spikes by showing that action potentials triggered by strong spikes were significantly more resistant to recurrent inhibition than those triggered by weak dendritic spikes (Figures 5A and 5B). Weak dendritic spike-triggered output, which on average was temporally delayed and more imprecise, was selectively inhibited by recurrent inhibition (Figures 5A, right panels, 5B). As a result of this temporal selectivity, the average action potential output had a significantly lower latency (median 5.0 ± 4.0 ms SD; n = 45 APs) in the presence of recurrent inhibition than under control conditions (median latency 11.1 ± 4.1 ms SD; n = 251 APs, Figures 5A and 5C). Notably, in comparison to control conditions, recruitment of recurrent inhibition resulted in a higher, relative contribution of strong dendritic spikes to action potential output (Figures 5A, lowest panel, and 5B).

Plasticity of Spike Sensitivity to Inhibition

Dendritic spike strength can undergo plasticity following either physiological theta rhythmic pairing of action potential output and dendritic spikes, or cholinergic modulation (Losonczy et al., 2008). We hypothesized that branch plasticity converting a weakly to a strongly spiking branch should effectively exempt this branch from inhibitory control. Therefore, we induced branch strength plasticity (BSP) in weakly spiking branches by pairing microiontophoretically induced dendritic spikes with action potential bursts evoked by somatic current injections (see Experimental Procedures). Following this stimulation paradigm the $\Delta V/\Delta t$ of the somatically recorded spikelets increased by 73% ± 25% (Figures 6A and 6B). To address whether a strengthening of weak dendritic spikes could provide an intrinsic mechanism counteracting recurrent inhibition, we compared the dendritic spike probability in the presence of recurrent inhibition

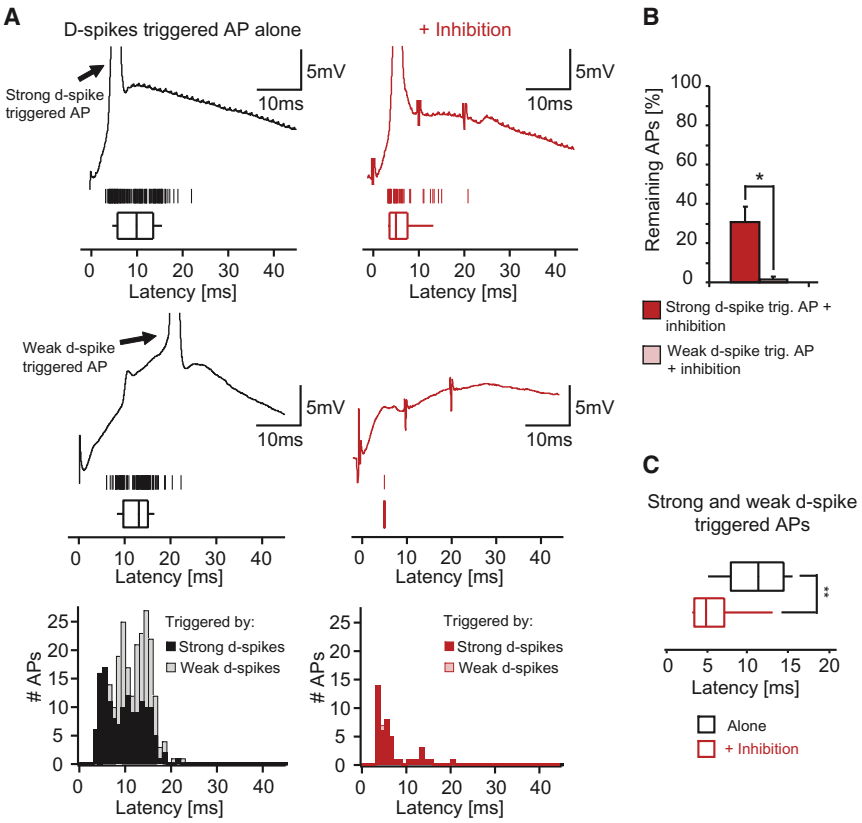

Figure 5. Selective Inhibition of Action Potentials Evoked by Weak Dendritic Spikes Results in a Numerically Reduced but More Precise CA1 Action Potential Output

(A) Upper row, black: example of strong dendritic spike-triggered AP, overall distribution and median of AP latencies without inhibition; red: strong dendritic spike-triggered AP recorded with recurrent inhibition, distribution and median of AP latencies. Middle row, black: same analysis for weak dendritic spike-triggered APs. Lower row: Latency histograms for all dendritic spike-triggered APs alone (black) and in the presence of recurrent inhibition (red).

(B) Remaining dendritic-spike-triggered APs in the presence of recurrent inhibition for strong (30.6% ± 8.0%, n = 10 cells) and weak (1.4% ± 1.2%; n = 8 cells) dendritic spike-triggered APs ($p < 0.05$; Mann-Whitney test); mean ± SEM.

(C) Box-plot for all dendritic spike (weak and strong spikes taken together)-triggered APs alone (black), and in the presence of recurrent inhibition (red; ANOVA and Dunnett post hoc; see Figure 7F); median ± SD.

before and after branch strength potentiation (Figures 6C–6E). Remarkably, already 8–10 min after the induction of branch strength potentiation weak dendritic spikes, which were initially inhibited (53% ± 10% reduction of dendritic spike probability), were strengthened to withstand recurrent inhibitory control (Figure 6E). After branch strength potentiation fast spikelet-triggered action potentials predominantly contributed to the overall dendritic spike dependent output (Figure 6F). We then tested if inhibition of subthreshold EPSPs is altered after induction of branch strength potentiation, suggesting an active downregulation of inhibition on a rapid timescale. We found that 8–10 min after induction of branch strength plasticity inhibition of subthreshold iEPSPs was not changed (iEPSP pre: 5.29mV ± 0.49mV; iEPSP post: 5.14mV ± 0.40mV; IPSP pre: −1.62mV ± 0.29mV; IPSP post: −1.70mV ± 0.31mV; n = 6; $p > 0.05$; Wilcoxon signed rank test; Figures 6G–6I). Thus, an exclusive increase in excitation provided by branch strength potentiation might be sufficient to permit inhibitory resistance.

Activity Dependence of Recurrent Inhibition

In some behavioral states an ensemble of CA1 pyramidal neurons fires rhythmically at theta frequency (O'Keefe and Nadel, 1978; Vanderwolf, 1969). Thus, we next tested if inhibitory control of excitatory signaling on proximal apical oblique or basal dendrites is attenuated, when recurrent inhibitory micronetworks are repeatedly activated at theta frequency (5 Hz; Figure 7A; see Figures S4E–S4G for other frequencies). We then visualized the dynamics of inhibition in the CA1 subfield using voltage sensitive dye imaging (Figures 7A, S4A, and S4B). A single burst stimulus applied to the alveus evoked a fast excitation in stratum pyramidale and stratum oriens, which was constant in amplitude during repeated burst stimulation at theta frequency (Figures S4B and S4C). Excitation was followed by an inhibitory signal, which extended spatially throughout all layers of the CA1 subfield (Figure 7A, left panel). Theta rhythmic repetition resulted in a significant reduction of the inhibitory signal in the stratum (str.) radiatum and str. oriens (75% ± 4% reduction, n = 10; $p < 0.01$; Wilcoxon signed rank test; Figures 7A, right panel, and 7B). In contrast, the inhibitory signal in str. lacunosum moleculare was persistent throughout the theta burst stimulation (Figure S7D).

The prominent reduction of recurrent inhibition in str. radiatum and oriens was also clearly reflected in a decrease of the compound IPSP amplitude recorded somatically in CA1 pyramidal neurons at theta frequencies (Figures S4D–S4G).

Whole-cell recordings revealed that interneurons with axonal projections within the str. radiatum and oriens predominantly received depressing input from CA1 pyramidal neurons (Figures S5A and S5B) and subsequently showed a theta-dependent reduction of firing probability (Figure S6). In contrast, interneurons projecting to str. lacunosum moleculare received predominantly facilitating input, resulting in a more persistent inhibition during theta rhythmic activity (Figures S5C, S5D, and S6).

Dynamic Regulation of Dendritic Linear and Nonlinear Excitation

We found that recurrent inhibition of iEPSPs evoked in str. oriens and radiatum was strongly reduced after theta rhythmic repetition (Figure S7C; 41% ± 5% inhibition compared to 22% ± 6% inhibition after repetition; n = 18; $p < 0.001$; Wilcoxon signed

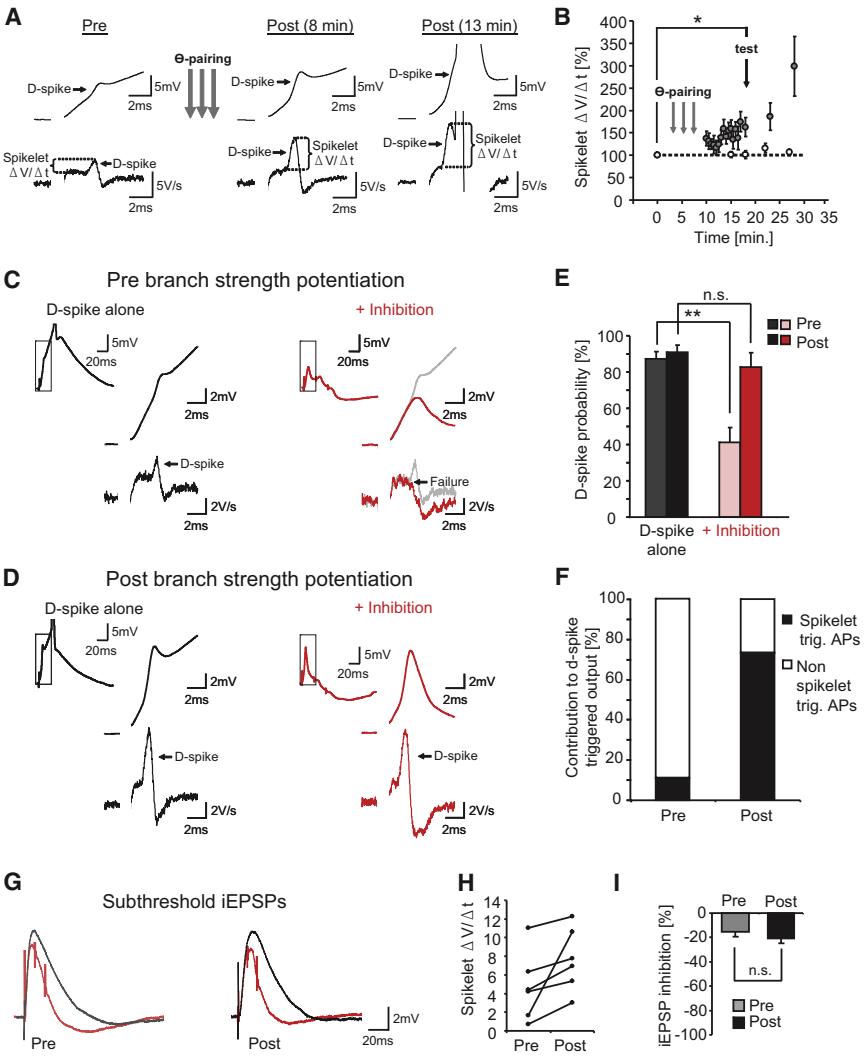

Figure 6. Branch Strength Plasticity Modulates Resistance of Dendritic Spikes to Inhibition

(A) Whole-cell recordings from CA1 pyramidal cells before (pre) and after (post) θ pairing protocol (see Experimental Procedures) to evoke branch strength plasticity. Left: dendritic spike and corresponding ΔV/Δt before (left) and 8 or 13 min after the pairing (right panels).

(B) Spikelet ΔV/Δt at sequential time points after the pairing normalized to control (before pairing). Significant increase in spikelet ΔV/Δt ($n = 9$, $p < 0.05$; Wilcoxon signed rank test). Open circles: ΔV/Δt of control dendritic spikes recorded without θ pairing ($n = 2–7$ branches); mean ± SEM.

(C) Example of a weak dendritic spike and corresponding ΔV/Δt alone (black) and in the presence of recurrent inhibition (red). Insets: lower magnification.

(D) Same dendritic spike after the pairing paradigm alone (black) and in the presence recurrent inhibition (red).

(E) Comparison of dendritic spiking probability alone (black) and with inhibition (red), before (light bars) and after branch strength potentiation (solid bars; dendritic spike probabilities for each branch were averaged, $n = 7$ initially weak branches; $p < 0.01$; Friedman/Dunn's test); mean ± SEM.

(F) Contribution of fast-spikelet-triggered (black) and nonspikelet-triggered (white) APs to overall dendritic spike-triggered output before and after pairing paradigm.

(G) Inhibition of subthreshold iEPSPs evoked on identified weakly or strongly excitable branches before and after branch strength potentiation.

(H) ΔV/Δt of somatically recorded spikelets for branches on which subthreshold iEPSPs were evoked before and after branch strength potentiation protocol.

(I) Percent inhibition of the same iEPSPs before and 10 min after branch strength potentiation ($p > 0.05$; $n = 6$; Wilcoxon signed rank test); mean ± SEM.

rank test). However, we observed an opposite dynamic regulation of excitatory events by recurrent inhibition in str. lacunosum moleculare. Here, recurrent inhibition failed to reduce local dendritic Ca^{2+} transients in response to the first stimulus but significantly reduced Ca^{2+} transients following repeated theta stimulation (Figure S7B). These dynamics are most likely a result of facilitating CA1 input on interneurons terminating in str. lacunosum moleculare (Figures S5, S6, and S7).

Does the dynamic reduction of recurrent inhibition regulate the generation of dendritic spikes in CA1 pyramidal neurons? We hypothesized that weak dendritic spikes, which are initially blocked by inhibition (Figures 3A–3F) could reoccur due to a rundown of inhibition during theta-patterned activity. Indeed, the initial block of weak dendritic spikes was lost following repetitive theta stimulation (Figures 7C and 7D). We found that the reoccurrence of weak dendritic spikes after the activity-dependent downregulation of recurrent inhibition resulted in a more numerous but on average less precise dendritic spike-triggered output (control: 251 APs with median latency: 11.1 ± 4.1 ms SD; first: 45 APs, latency: 5.0 ± 4.0 ms SD; repeated stimulation: 116 APs, latency: 8.1 ± 8.5 ms SD; Figures 7E and 7F).

This theta dynamic inhibitory regulation of linear and nonlinear excitatory integration suggests that input/output coupling provided by dendritic spikes may strongly depend on the pattern of ongoing network activity.

DISCUSSION

In this study we investigated how recurrent inhibition, provided by hippocampal inhibitory microcircuits, regulates the integration of EPSPs and dendritic spikes in CA1 pyramidal neurons. Our data reveal that the effectiveness of recurrent inhibition depends on the dendritic excitatory input pattern and the intrinsic excitability of dendritic branches. On dendritic branches exhibiting weak excitability, local inputs evoked EPSPs and weak dendritic spikes. These were reliably suppressed by recurrent inhibition. In contrast, strong dendritic spikes evoked on

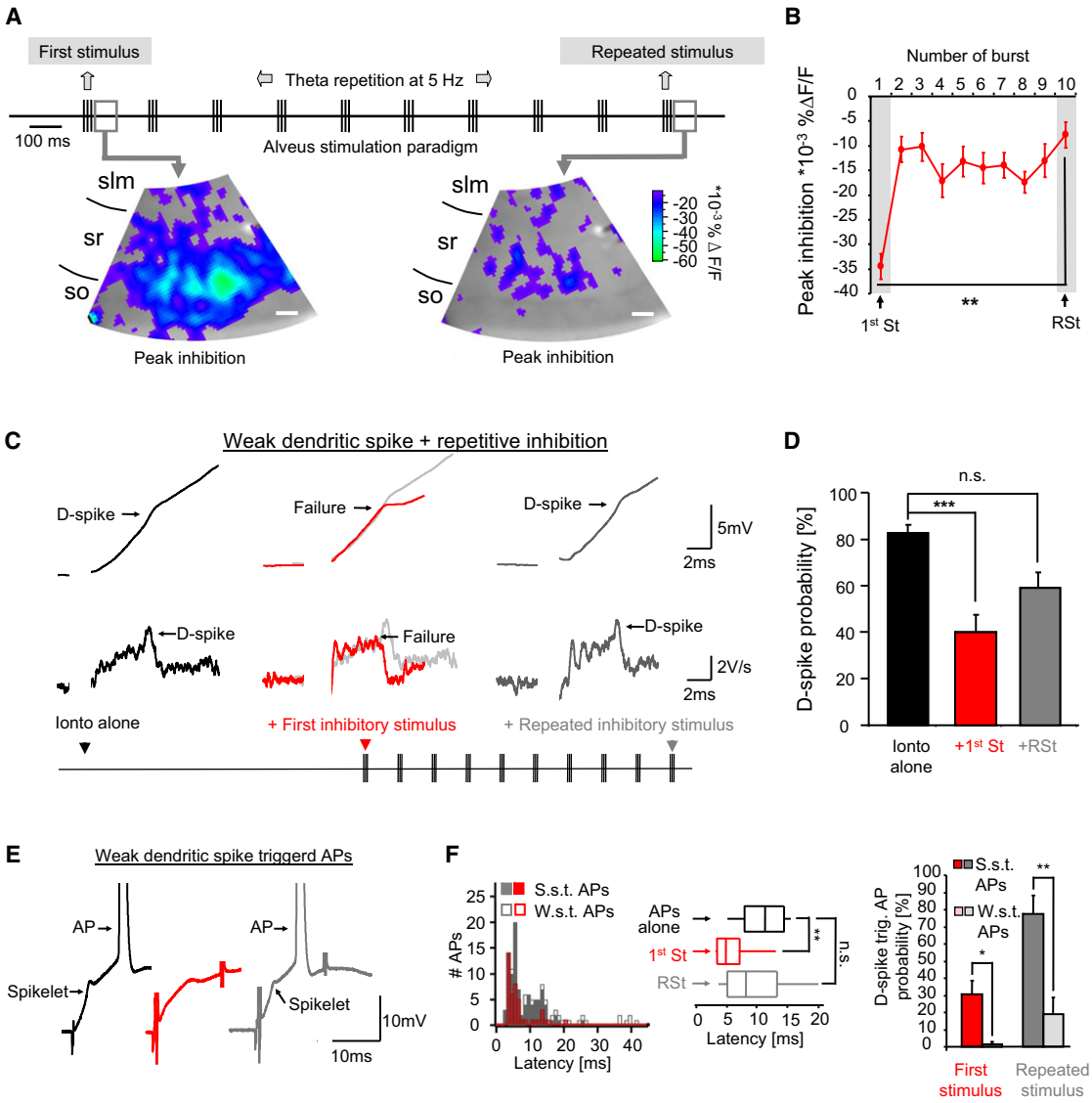

Figure 7. Theta-Dependent Reduction of Recurrent Inhibition Regulates Dendritic Spike Generation and Neuronal Output

(A) Voltage imaging using di-3-ANEPPDHQ dye and 1 kHz CCD image acquisition: inhibitory signal across the CA1 subfield in response to alveus-stimulation. Left: voltage signal in response to the first burst. Right: inhibitory voltage signal in response to a theta-repeated burst. Scale bars represent 200 μm.

(B) Time course of inhibitory signal in response to θ repetition of the burst stimulus. Average inhibitory signal in the Schaffer-collateral integration zone (so and sr; n = 10 slices; $p < 0.01$; Wilcoxon signed rank test); mean ± SEM.

(C) Representative example of a weak dendritic spike alone (black) and with recurrent inhibition activated by a single (red) or a repeated stimulus (gray).

(D) Bar graph represents dendritic spike probabilities (weak dendritic spikes, n = 14; $p < 0.001$, Friedman and Dunn's post hoc test).

(E) Example of a weak dendritic spike-triggered AP alone (black), together with the first (red) or repeated inhibitory event; mean ± SEM.

(F) Latency histogram of all dendritic spike-triggered APs (weak: open bars and strong: solid bars) in the presence of the first (red) and the repeated stimulus (gray). Middle panel: dendritic spike-triggered APs latencies alone (black) and in the presence of the first (red) and the repeated stimulus (gray; ANOVA and Dunnett post hoc test); median ± SD. Right panel: percent remaining dendritic spike-triggered APs in the presence of recurrent inhibition for weak dendritic spike-triggered APs (W.s.t. APs) and strong dendritic spike-triggered APs (S.s.t. APs, Mann-Whitney test); mean ± SEM. See also Figures S4, S5, S6, and S7.

branches with high intrinsic excitability resisted recurrent inhibition and therefore provided persistent input-output coupling. Furthermore, we found that plasticity of branch excitability enabled weakly excitable branches to increase their resistance to inhibition.

A Specialized Role of Strong Dendritic Spikes in the Presence of Inhibition

Previous studies on excitatory signal integration have shown that dendritic spikes amplify spatially and temporally correlated inputs from presynaptic ensembles and consequently facilitate

the conversion of these inputs to an action potential output (Gasparini et al., 2004; Losonczy and Magee, 2006; Remy et al., 2009; Stuart et al., 1997). Our experiments now show that the activation of recurrent inhibition significantly reduces the set of dendritic branches that are able to generate dendritic spike-triggered action potential output. We show that inhibition virtually excluded dendritic branches on which weak spikes and EPSPs were generated from direct triggering of action potential output.

In contrast, strong dendritic spikes converted correlated branch input to highly precise, spikelet-triggered action potential output despite the presence of recurrent inhibition. This resistance was not only present when recurrent synapses were selectively activated, but also when local branch inhibition was evoked using GABA microiontophoresis, which is not selective for either recurrent or feedforward circuits. Resistance to inhibition was also not restricted to a specific timing of excitation and inhibition, an observation suggesting that strong dendritic spikes may also withstand feedforward activation of dendritic inhibitory synapses. Indeed, some dendrite targeting interneuron subtypes participating in recurrent inhibition have been shown to also be recruited by CA3-Schaffer collateral input in a feedforward manner (Somogyi and Klausberger, 2005). The interaction of inhibitory synapses with dendritic excitation and spike generation provided by these subtypes was not a direct focus of this study, but in our experiments feedforward inhibitory synapses were coactivated with recurrent synapses when we performed GABA microiontophoresis on a branch.

By exhibiting resistance to recurrent inhibition strong dendritic spikes may ensure effective input to output coupling for correlated inputs on highly excitable dendritic branches, whereas weakly spiking dendrites become much less effective. Thus, inhibition segregates branches, and their presynaptic afferent assemblies, into two distinct populations based on their output efficacy. Notably, the concept of input feature detection by active dendrites is still applicable (Losonczy et al., 2008), but in the presence of inhibition applies to the much more limited set of strongly spiking dendrites that subsequently are capable of providing precisely timed output.

Why are strong spikes more resistant to inhibition? The most straightforward explanation is that the stronger depolarization resulting from a functional downregulation of local A-type potassium channels (Losonczy et al., 2008) more effectively bypasses the voltage gap and shunt provided by dendritic inhibition. Several lines of evidence suggest that this is the case. First, EPSP summation, depolarization evoked by dendritic current injection, and local dendritic Ca^{2+} increase have been shown to be stronger, when A-type potassium channels were pharmacologically blocked (Cash and Yuste, 1999; Hoffman et al., 1997; Losonczy and Magee, 2006). Second, computational modeling suggests that in the dendritic compartment any amount of inhibition can be overcome by further excitation since local inhibition prevents excitatory saturation (Vu and Krasne, 1992). Thus, an exclusive increase in excitation might be sufficient to permit inhibitory resistance without selective changes in inhibition.

Interestingly, we detected a weaker recurrent inhibition of subthreshold EPSPs evoked on strong branches, suggesting an additional mechanism, which may contribute. Such a supplementary mechanism could result from a branch specific adaptation of GABAergic synaptic efficacy. Several mechanisms for the regulation of GABAergic efficacy have been proposed, which could act on single branch level. They include a different functional expression or density of GABA receptors (Luscher et al., 2011) and a local modification of the GABA reversal potential (Földy et al., 2010; Lee et al., 2011; Rivera et al., 2004; Woodin et al., 2003). However, our experiments revealed that postsynaptic mechanisms were not likely to participate, since we neither found evidence for differences in branch GABA conductance nor significant changes in the local GABA reversal potential. Other putatively presynaptic mechanisms involving a retrograde messenger molecule or LTD of inhibitory synapses have to be explored further, but were clearly not in the scope of this study.

Role of Branch Strength Plasticity in Controlling the Efficacy of Inhibition

We have demonstrated the existence of a plasticity mechanism that can convert weakly excitable to strongly excitable branches, as was shown in a previous study (Losonczy et al., 2008). It is readily induced by repeatedly eliciting dendritic spikes together with backpropagating action potentials. A key mechanism underlying this form of plasticity is an NMDA receptor-dependent downregulation of A-type potassium channels (Losonczy et al., 2008).

We showed that branch strength potentiation provides a plasticity mechanism that can render individual branches insensitive to recurrent inhibition. This implies that any dendritic branch exhibiting nonlinear excitability could potentially gain resistance to inhibition on a rapid timescale, if the conditions for branch strength potentiation are fulfilled. Inhibition of subthreshold EPSPs was unaltered suggesting that GABAergic efficacy is regulated on an intermediate or longer timescale. Alternatively, plasticity of inhibitory synapses could be mechanistically involved, which is unlikely to be induced by the pairing protocol used in this study, since it does lead to activation of presynaptic interneurons. So far, our data suggest that an increase in excitation provided by branch strength potentiation can be sufficient to permit resistance to recurrent inhibition, but plasticity of inhibitory synapses cannot be excluded.

In our experiments branch strength potentiation could be elicited, when somatic action potentials occurred simultaneously with correlated branch inputs. In vivo, these conditions could be met in sharp-waves, where up to 10% of coactivated presynaptic CA3 neurons excite CA1 pyramidal neurons by simultaneously activating at least several tens of excitatory synapses within a narrow time window of less than 20 ms (Csicsvari et al., 2000).

These phenomena are intriguing because they are branch-specific, and thus affect output generation predominantly from presynaptic cell assemblies projecting in a topographically organized manner to individual branches.

In addition to branch plasticity, a number of other plasticity mechanisms might contribute to produce branch-specific structuring of input patterns. For example, sensory experience causes plastic enrichment of GluR1 AMPA receptor subunits in groups of closely adjacent spines on individual branches. This indicates an LTP-like plasticity phenomenon evoked in vivo, and might

result in branch-specific potentiation of excitatory transmission (Kleindienst et al., 2011; Makino and Malinow, 2011). It is intriguing to speculate that if LTP would occur in a cluster of synapses restricted to a branch, it could be functionally linked to downregulation of voltage-gated A-type potassium channels (Frick et al., 2004) and therefore permit inhibitory resistance to any dendritic spike locally evoked by these synapses.

Impact of Recurrent Inhibition Is Dynamic

The recurrent inhibitory microcircuitry constrains the temporal precision of EPSP-driven action potentials via recruitment of interneurons (Miles, 1990). We now demonstrate that recurrent inhibition strongly regulates the contribution of not only EPSPs, but also of weak dendritic spikes to action potential output. We show that this inhibitory control is highly dependent on ongoing network activity, as recurrent inhibition within the str. radiatum and oriens undergoes a strong, dynamic reduction when CA1 pyramidal neurons are recruited into network activity at frequencies of 5–10 Hz.

These data have implications for excitatory-inhibitory interactions in vivo. If the CA1 neuronal ensembles discharge within a period of sparse background activity, recurrent inhibition would be expected to provide strong inhibition of proximal inputs. Such episodes of sparse background activity of CA1 neurons can be particularly observed during slow-wave sleep and awake immobility (O'Neill et al., 2006; Thompson and Best, 1989; Ylinen et al., 1995), but intermittent periods of reduced CA1 ensemble firing rates of 1 Hz and below may also occur during other states of network activity (Thompson and Best, 1989). On the other hand, during theta rhythmic ensemble activity that occurs during explorative behavior and rapid-eye-movement sleep (O'Keefe and Nadel, 1978), CA1 pyramidal neurons repetitively discharge single or bursts of action potentials at frequencies of 4–12 Hz (Csicsvari et al., 1999; Ranck, 1973). Under these conditions, our data predict a strong attenuation of proximal inhibition already after the first few theta cycles, and a concomitantly higher contribution of weak dendritic spikes and EPSPs to action potential output. A further corollary of the theta-induced decrease of inhibition would be a degraded output precision, since in addition to strong dendritic spikes, now temporally more variable EPSPs and weak dendritic spikes contribute to action potential output. This observation implies that during theta activity of CA1 ensembles more branches can efficiently contribute to output. The increase in output probability caused by a decrease in recurrent inhibition is consistent with the elevated firing frequency of the CA1 ensemble during exploration observed in vivo (Thompson and Best, 1989).

Our data suggest that the perforant path input is less strongly regulated by recurrent inhibition, when compared to Schaffer collateral input. However, repetitive CA1 pyramidal neuron activity at theta frequency resulted in a mildly augmented local inhibition observed with two-photon calcium imaging. Therefore, the proper integration of both, perforant path and Schaffer collateral excitatory inputs during theta activity, which is thought to be critically relevant for long-term spatial memory consolidation (Remondes and Schuman, 2002, 2004), may depend on the differential recruitment of recurrent interneurons (Pouille and Scanziani, 2004).

Taken together, the input to output coupling of CA1 pyramidal neurons is controlled by an activity-dependent regulation of recurrent inhibition, which may be observed during different network activities in vivo. Furthermore we identify a mechanism, by which correlated input on dendritic branches could resist inhibitory control, which is widely independent of the network activity patterns: In both, periods of sparse and periods of higher rhythmic network activity, the generation and plasticity of dendritic spikes may serve to reliably couple the information conveyed by the activity of a presynaptic cell assembly to precise CA1 action potential output.

EXPERIMENTAL PROCEDURES

Slice Preparation and Electrophysiology

Male Wistar rats (P21–P28, Charles River, Germany) were deeply anesthetized with an injection of ketamine (100 mg/kg, Pfizer, Germany) and xylazine (15 mg/kg; Bayer, Leverkusen, Germany) and then decapitated. The brain was quickly transferred to ice cold artificial sucrose-based cerebrospinal fluid ($ACSF_{sucrose}$) containing (in mM): 60 NaCl, 100 sucrose, 2.5 KCl, 1.25 NaH_2PO_4, 26 $NaHCO_3$, 1 $CaCl_2$, 5 $MgCl_2$, 20 glucose. Slices (300 μm thick) were cut with a vibratome (Leica, Wetzlar, Germany) and incubated in $ACSF_{sucrose}$ at 35°C for 30 min. Subsequently slices were transferred to a submerged holding chamber containing normal ACSF solution (in mM: 125 NaCl, 3 KCl, 1.25 NaH_2PO_4, 26 $NaHCO_3$, 2.6 $CaCl_2$, 1.3 $MgCl_2$, 15 glucose) at room temperature. All extracellular solutions were constantly carbogenized (95% O_2, 5% CO_2). Since $GABA_B$ receptors play only a minor role in the inhibition mediated by the recurrent inhibitory network in CA1 (Alger and Nicoll, 1982a, 1982b; Newberry and Nicoll, 1984), $GABA_B$ receptors were blocked with 1 μM CGP55845 (Tocris) in all experiments.

Current-clamp whole-cell recordings were performed at 34 ± 1°C using a DAGAN (BVC-700A) or Multiclamp 700B amplifier (Molecular Devices, Union City, CA) at a 100 kHz sampling rate using a Digidata (1322A, Axon Instruments) interface controlled by pClamp Software (Molecular Devices). Recording pipettes were pulled with a vertical puller (Narishige PP-830) to 3–5 MΩ resistance resulting in series resistance ranging from 8–25 MΩ. To visualize dendrites we used a water immersion objective (Olympus 60×/NA0.9, Tokyo, Japan) on either a two-photon laser scanning microscope (TRIM Scope II; LaVision Biotec, Bielefeld, Germany) or on a Zeiss Axioskop 2 FS upright microscope with Dodt-contrast infrared illumination (TILLPhotonics, Gräfelfing, Germany). In the latter experimental setup, a monochromator with an integrated light source (TILLPhotonics) was used to excite intracellular Alexa Fluor 488 (Invitrogen). To minimize photo damage during imaging we synchronized acquisition and illumination by repetitively triggering the light source (exposure times ranged from usually 10 to a maximum of 30 ms).

Most whole-cell recordings were performed using an intracellular solution resembling a physiological chloride driving force (in mM: 140 K-gluconate, 7 KCl, 5 HEPS-acid, 0.5 $MgCl_2$, 5 phosphocreatine, 0.16 EGTA). In some recordings (Figures 2A, S4D–S4G, S6A, and S6B) a lower intracellular Cl^- concentration (1 mM) was used.

The cell-attached recordings were conducted with an Axopatch 200B amplifier (Molecular Devices) in voltage-clamp mode and patch pipettes (5–7 MΩ resistance) were filled with normal ACSF.

To exclusively recruit the recurrent inhibitory interneuron population we electrically stimulated the CA1 pyramidal cell axons in the alveus. To achieve an isolated stimulation of CA1 axons we cut off the subiculum sparing the alveus. In addition, the CA3 subfield was separated. We placed a cluster electrode (CE2F75; FHC, Bowdoin, ME) onto the alveus on the subicular side of the cut and applied 10 (or 15 in some experiments) biphasic current pulses (0.15–0.2 ms, 0.01–0.3 mA) in 100 Hz bursts at theta frequency (5 Hz). To generate the current pulses we used a stimulus isolator (A-M Systems, Model 2100).

During theta pairing protocol three dendritic spikes were evoked at 200 ms intervals. The first two dendritic spikes were elicited together with three short somatic current injections (5 ms, 900 pA) resulting in a burst of two to three

action potentials. The third dendritic spike was used as a control to determine whether the microiontophoretic glutamate pulse was reliably initiating dendritic spikes. This pairing protocol was repeated 15 times with a 30 s interval. The whole stimulation paradigm was then repeated three times with a 5 min interval between the repetitions (Losonczy et al., 2008).

All animal experiments were conducted in accordance with the guidelines of the Animal Care and Use Committee of the University of Bonn.

Fluorescent Interneuron Staining and Confocal Imaging

The interneurons were recorded with intracellular solution (see above) containing 0.3%–0.5% biocytin (Sigma). After the experiment slices were transferred to 4% paraformaldehyde (PFA) for 12 hr. For fluorescent staining and post hoc reconstruction of the axonal arbor the slices were washed with 0.1 M phosphate-buffer (PB, pH 7.4) and tris-buffered salt solution (TBS) at room temperature. Subsequently, slices were incubated with Streptavidin Alexa Fluor 488 (1:500) conjugate (Invitrogen) in TBS for 2 hr in the dark. After washing the slices thoroughly in 0.1 M PB they were embedded in Vectashield mounting medium (Vector Labs) and kept at 4°C in the dark. Confocal image planes were acquired with a confocal microscope (DM RBE, Leica, Wetzlar, Germany) using Leica imaging software (Leica Confocal Software 2.00). Maximum intensity projections of confocal image stacks were performed with ImageJ (NIH). Axonal arborization was reconstructed using Adobe Photoshop CS5.

Fast CCD Voltage Imaging

To visualize voltage changes of excitable membranes in the CA1 field, 350 μm slices were kept in an interface-chamber and incubated with 100 μM of the naphthylstyryl-pyridinium dye, di-3-ANEPPDHQ ($C_{30}H_{43}Br_2N_3O_2$; Invitrogen) in ACSF for 15 min before the experiment. While stimulating the recurrent interneuronal population with the alveus-stimulation (described above) we acquired epifluorescence with a fast CCD camera at 1 kHz frame rate (80 × 80 pixels, NeuroCCD; RedShirtImaging, Fairfield, CT). The fluorescent dye was exited using a 150 W xenon lamp driven by a stable power supply (Opti Quip, Highland Mills, NY). Theta burst protocol was applied 0.5 s after the start of image acquisition to exclude mechanical noise resulting from shutter opening. We acquired images of the whole CA1 subfield by using a low magnification objective (XLFLUOR 4×, 0.28 NA; Olympus, Tokyo, Japan). All technical instruments were switched on at least 30 min before recordings to avoid thermal drift. Voltage signals were recorded at 34°C ± 1°C (Ang et al., 2005; Carlson and Coulter, 2008). Data were analyzed using custom-made routines in IGOR PRO (Wavemetrics, Lake Oswego, OR). Correction for bleaching was warranted by subtracting a double exponential fit of the traces (Figure S4B). Peak changes in fluorescence (% ΔF/F) of excitatory signals (fast, negative peaks) were obtained in a 50 ms time window during stimulation. Peak inhibitory signals (slower, positive peaks) were obtained in a 160 ms time window after the excitatory signal. The average fluorescence 20 ms before stimulation was used as baseline. Values were multiplied by −1 resulting in excitatory events being represented by positive values and inhibitory events by negative values. The range displayed in the pseudocolor images was set from -12×10^{-3}% ΔF/F to -100×10^{-3}% ΔF/F and spatially smoothed (3 × 3 pixels).

Glutamate and GABA Microiontophoresis

Fine, high resistance electrodes (40–90 MΩ) were pulled with a horizontal puller (P-97; Sutter Instrument Company, Novato, CA) and filled with 150 mM glutamatic acid (pH was adjusted to 7.0 with NaOH) and 50 μM Alexa Fluor 488 or 594 hydrazide (Invitrogen) for visualization. We used a microiontophoresis system (MVCS-02; NPI Electronic, Tamm, Germany) with capacitance compensation. The pipette tip was placed close to the dendrite <1 μm and short negative current pulses (0.1–0.4 ms, 0.01–1 μA) were applied to eject glutamate and evoke iEPSPs, dendritic spikes, and action potentials (Murnick et al., 2002).

Similar settings were used for GABA microiontophoresis except a positive a current was applied to eject GABA. To achieve a positive charge of GABA in the 1 M GABA solution, the pH was adjusted to 5 with HCl (Pugh and Jahr, 2011). When GABA microiontophoresis was combined with dendritic spike initiation the timing of inhibition was adjusted to the time point of maximal inhibitory effect.

In alveus stimulation experiments we applied the iontophoretic current and the alveus stimulation synchronously (t_0) to achieve a physiological timing of excitation and recurrent inhibition. In this case, the onset of the iEPSP preceded the onset of recurrent inhibition, which was disynaptically delayed. In some experiments (Figures 3E–3H), excitation was timed to occur closer to the peak of recurrent inhibition (t_1: 20 ms delayed and t_2: 50 ms delayed).

Two-Photon Ca^{2+} Imaging

We imaged Ca^{2+}-signals from small caliber dendrites of CA1 pyramidal cells using two-photon excitation of Oregon Green BAPTA 1 (OGB1, Invitrogen) and Alexa 594 at a wavelength of 820 nm using a Ti:Sapphire ultrafast-pulsed laser (Chameleon Ultra II, Coherent) and a galvanometer-based scanning system (Prairie Technologies, Middleton, WI) on an Olympus BX51 upright microscope with a high NA objective (60×, 0.9 NA; Olympus). Cells were patched with the standard intracellular solution, additionally containing 200 μM of the high affinity Ca^{2+} indicator OGB1 and 50 μM Alexa Fluor 594. EGTA was not included in Ca^{2+} imaging experiments. Linescans were performed on the dendrites of interest with a frequency ≥420 Hz. From the raw fluorescence the normalized change in fluorescence (%ΔF/F) was calculated using a time period of 100 ms before stimulation onset as baseline.

Data Analysis and Statistics

Electrophysiological data was recorded using Clampex 9.0 software (Molecular Devices) and analyzed with IGOR PRO (Wavemetrics, Lake Oswego, OR), Clampfit 10.0 (Molecular Devices), and Excel (Microsoft, Redmond, WA). Peak ΔV/Δt values of the dendritic spikes were obtained from the first derivative of the boxcar-filtered (23 smoothing points) voltage trace (Remy et al., 2009). All results are given as mean ± SEM, if not indicated otherwise. Dendritic spike and AP probabilities were determined for each cell and then averaged. Statistical significance was tested using appropriate tests in Prism4 (GraphPad Software, San Diego, CA). The statistical tests used are indicated in the figure legends.

SUPPLEMENTAL INFORMATION

Supplemental Information includes seven figures and can be found with this article online at http://dx.doi.org/10.1016/j.neuron.2012.06.025.

ACKNOWLEDGMENTS

We thank R. Krueppel and N. Spruston for helpful comments on the manuscript. We are also grateful to I. Soltesz and D. Feldmayer for assistance with interneuron staining. We thank the DZNE microscopy facility and F. Fuhrmann for technical support. This work was supported by the ministry of research MIWF of the state Northrhine-Westfalia (S.R.), ERA-Net Neuron (S.R. and H.B.), the BMBF-Projekträger DLR US-German collaboration in computational neuroscience (CRCNS; S.R.), Centers of Excellence in Neurodegenerative Diseases (COEN; S.R.), and the University of Bonn intramural funding program (BONFOR; S.R.).

Accepted: June 8, 2012
Published: September 5, 2012

REFERENCES

Alger, B.E., and Nicoll, R.A. (1982a). Feed-forward dendritic inhibition in rat hippocampal pyramidal cells studied in vitro. J. Physiol. *328*, 105–123.

Alger, B.E., and Nicoll, R.A. (1982b). Pharmacological evidence for two kinds of GABA receptor on rat hippocampal pyramidal cells studied in vitro. J. Physiol. *328*, 125–141.

Ali, A.B., and Thomson, A.M. (1998). Facilitating pyramid to horizontal oriens-alveus interneurone inputs: dual intracellular recordings in slices of rat hippocampus. J. Physiol. *507*, 185–199.

Ali, A.B., Deuchars, J., Pawelzik, H., and Thomson, A.M. (1998). CA1 pyramidal to basket and bistratified cell EPSPs: dual intracellular recordings in rat hippocampal slices. J. Physiol. *507*, 201–217.

Ang, C.W., Carlson, G.C., and Coulter, D.A. (2005). Hippocampal CA1 circuitry dynamically gates direct cortical inputs preferentially at theta frequencies. J. Neurosci. *25*, 9567–9580.

Antic, S., Major, G., and Zecevic, D. (1999). Fast optical recordings of membrane potential changes from dendrites of pyramidal neurons. J. Neurophysiol. *82*, 1615–1621.

Ariav, G., Polsky, A., and Schiller, J. (2003). Submillisecond precision of the input-output transformation function mediated by fast sodium dendritic spikes in basal dendrites of CA1 pyramidal neurons. J. Neurosci. *23*, 7750–7758.

Carlson, G.C., and Coulter, D.A. (2008). In vitro functional imaging in brain slices using fast voltage-sensitive dye imaging combined with whole-cell patch recording. Nat. Protoc. *3*, 249–255.

Cash, S., and Yuste, R. (1999). Linear summation of excitatory inputs by CA1 pyramidal neurons. Neuron *22*, 383–394.

Csicsvari, J., Hirase, H., Czurkó, A., Mamiya, A., and Buzsáki, G. (1999). Oscillatory coupling of hippocampal pyramidal cells and interneurons in the behaving Rat. J. Neurosci. *19*, 274–287.

Csicsvari, J., Hirase, H., Mamiya, A., and Buzsáki, G. (2000). Ensemble patterns of hippocampal CA3-CA1 neurons during sharp wave-associated population events. Neuron *28*, 585–594.

Ferster, D., and Jagadeesh, B. (1992). EPSP-IPSP interactions in cat visual cortex studied with in vivo whole-cell patch recording. J. Neurosci. *12*, 1262–1274.

Földy, C., Lee, S.H., Morgan, R.J., and Soltesz, I. (2010). Regulation of fast-spiking basket cell synapses by the chloride channel ClC-2. Nat. Neurosci. *13*, 1047–1049.

Freund, T.F., and Buzsáki, G. (1996). Interneurons of the hippocampus. Hippocampus *6*, 347–470.

Frick, A., Magee, J., and Johnston, D. (2004). LTP is accompanied by an enhanced local excitability of pyramidal neuron dendrites. Nat. Neurosci. *7*, 126–135.

Gasparini, S., Migliore, M., and Magee, J.C. (2004). On the initiation and propagation of dendritic spikes in CA1 pyramidal neurons. J. Neurosci. *24*, 11046–11056.

Golding, N.L., and Spruston, N. (1998). Dendritic sodium spikes are variable triggers of axonal action potentials in hippocampal CA1 pyramidal neurons. Neuron *21*, 1189–1200.

Golding, N.L., Staff, N.P., and Spruston, N. (2002). Dendritic spikes as a mechanism for cooperative long-term potentiation. Nature *418*, 326–331.

Halasy, K., Buhl, E.H., Lörinczi, Z., Tamás, G., and Somogyi, P. (1996). Synaptic target selectivity and input of GABAergic basket and bistratified interneurons in the CA1 area of the rat hippocampus. Hippocampus *6*, 306–329.

Hao, J., Wang, X.D., Dan, Y., Poo, M.M., and Zhang, X.H. (2009). An arithmetic rule for spatial summation of excitatory and inhibitory inputs in pyramidal neurons. Proc. Natl. Acad. Sci. USA *106*, 21906–21911.

Hoffman, D.A., Magee, J.C., Colbert, C.M., and Johnston, D. (1997). K^+ channel regulation of signal propagation in dendrites of hippocampal pyramidal neurons. Nature *387*, 869–875.

Holthoff, K., Kovalchuk, Y., Yuste, R., and Konnerth, A. (2004). Single-shock LTD by local dendritic spikes in pyramidal neurons of mouse visual cortex. J. Physiol. *560*, 27–36.

Kleindienst, T., Winnubst, J., Roth-Alpermann, C., Bonhoeffer, T., and Lohmann, C. (2011). Activity-dependent clustering of functional synaptic inputs on developing hippocampal dendrites. Neuron *72*, 1012–1024.

Koch, C., Poggio, T., and Torre, V. (1983). Nonlinear interactions in a dendritic tree: localization, timing, and role in information processing. Proc. Natl. Acad. Sci. USA *80*, 2799–2802.

Lee, H.H., Deeb, T.Z., Walker, J.A., Davies, P.A., and Moss, S.J. (2011). NMDA receptor activity downregulates KCC2 resulting in depolarizing $GABA_A$ receptor-mediated currents. Nat. Neurosci. *14*, 736–743.

Losonczy, A., and Magee, J.C. (2006). Integrative properties of radial oblique dendrites in hippocampal CA1 pyramidal neurons. Neuron *50*, 291–307.

Losonczy, A., Makara, J.K., and Magee, J.C. (2008). Compartmentalized dendritic plasticity and input feature storage in neurons. Nature *452*, 436–441.

Luscher, B., Fuchs, T., and Kilpatrick, C.L. (2011). GABAA receptor trafficking-mediated plasticity of inhibitory synapses. Neuron *70*, 385–409.

Makara, J.K., Losonczy, A., Wen, Q., and Magee, J.C. (2009). Experience-dependent compartmentalized dendritic plasticity in rat hippocampal CA1 pyramidal neurons. Nat. Neurosci. *12*, 1485–1487.

Makino, H., and Malinow, R. (2011). Compartmentalized versus global synaptic plasticity on dendrites controlled by experience. Neuron *72*, 1001–1011.

McBain, C.J., and Fisahn, A. (2001). Interneurons unbound. Nat. Rev. Neurosci. *2*, 11–23.

Miles, R. (1990). Synaptic excitation of inhibitory cells by single CA3 hippocampal pyramidal cells of the guinea-pig in vitro. J. Physiol. *428*, 61–77.

Miles, R., Tóth, K., Gulyás, A.I., Hájos, N., and Freund, T.F. (1996). Differences between somatic and dendritic inhibition in the hippocampus. Neuron *16*, 815–823.

Milojkovic, B.A., Radojicic, M.S., Goldman-Rakic, P.S., and Antic, S.D. (2004). Burst generation in rat pyramidal neurones by regenerative potentials elicited in a restricted part of the basilar dendritic tree. J. Physiol. *558*, 193–211.

Murnick, J.G., Dubé, G., Krupa, B., and Liu, G. (2002). High-resolution iontophoresis for single-synapse stimulation. J. Neurosci. Methods *116*, 65–75.

Newberry, N.R., and Nicoll, R.A. (1984). A bicuculline-resistant inhibitory postsynaptic potential in rat hippocampal pyramidal cells in vitro. J. Physiol. *348*, 239–254.

O'Keefe, J., and Nadel, L. (1978). The hippocampus as a cognitive map (Oxford: Clarendon Press).

O'Neill, J., Senior, T., and Csicsvari, J. (2006). Place-selective firing of CA1 pyramidal cells during sharp wave/ripple network patterns in exploratory behavior. Neuron *49*, 143–155.

Pouille, F., and Scanziani, M. (2004). Routing of spike series by dynamic circuits in the hippocampus. Nature *429*, 717–723.

Pugh, J.R., and Jahr, C.E. (2011). Axonal $GABA_A$ receptors increase cerebellar granule cell excitability and synaptic activity. J. Neurosci. *31*, 565–574.

Ranck, J.B., Jr. (1973). Studies on single neurons in dorsal hippocampal formation and septum in unrestrained rats. I. Behavioral correlates and firing repertoires. Exp. Neurol. *41*, 461–531.

Remondes, M., and Schuman, E.M. (2002). Direct cortical input modulates plasticity and spiking in CA1 pyramidal neurons. Nature *416*, 736–740.

Remondes, M., and Schuman, E.M. (2004). Role for a cortical input to hippocampal area CA1 in the consolidation of a long-term memory. Nature *431*, 699–703.

Remy, S., and Spruston, N. (2007). Dendritic spikes induce single-burst long-term potentiation. Proc. Natl. Acad. Sci. USA *104*, 17192–17197.

Remy, S., Csicsvari, J., and Beck, H. (2009). Activity-dependent control of neuronal output by local and global dendritic spike attenuation. Neuron *61*, 906–916.

Rivera, C., Voipio, J., Thomas-Crusells, J., Li, H., Emri, Z., Sipilä, S., Payne, J.A., Minichiello, L., Saarma, M., and Kaila, K. (2004). Mechanism of activity-dependent downregulation of the neuron-specific K-Cl cotransporter KCC2. J. Neurosci. *24*, 4683–4691.

Schiller, J., Major, G., Koester, H.J., and Schiller, Y. (2000). NMDA spikes in basal dendrites of cortical pyramidal neurons. Nature *404*, 285–289.

Somogyi, P., and Klausberger, T. (2005). Defined types of cortical interneurone structure space and spike timing in the hippocampus. J. Physiol. *562*, 9–26.

Stokes, C.C., and Isaacson, J.S. (2010). From dendrite to soma: dynamic routing of inhibition by complementary interneuron microcircuits in olfactory cortex. Neuron *67*, 452–465.

Stuart, G., Schiller, J., and Sakmann, B. (1997). Action potential initiation and propagation in rat neocortical pyramidal neurons. J. Physiol. *505*, 617–632.

Thompson, L.T., and Best, P.J. (1989). Place cells and silent cells in the hippocampus of freely-behaving rats. J. Neurosci. *9*, 2382–2390.

Vanderwolf, C.H. (1969). Hippocampal electrical activity and voluntary movement in the rat. Electroencephalogr. Clin. Neurophysiol. *26*, 407–418.

Vu, E.T., and Krasne, F.B. (1992). Evidence for a computational distinction between proximal and distal neuronal inhibition. Science *255*, 1710–1712.

Woodin, M.A., Ganguly, K., and Poo, M.M. (2003). Coincident pre- and postsynaptic activity modifies GABAergic synapses by postsynaptic changes in Cl^- transporter activity. Neuron *39*, 807–820.

Ylinen, A., Bragin, A., Nádasdy, Z., Jandó, G., Szabó, I., Sik, A., and Buzsáki, G. (1995). Sharp wave-associated high-frequency oscillation (200 Hz) in the intact hippocampus: network and intracellular mechanisms. J. Neurosci. *15*, 30–46.